Communication

Not peer-reviewed version

Periodical Ultramodulation of Broadened Laser Spectra in Diamond at Variable Ultrashort Laser Pulsewidths: Ultrafast Plasma, Plasmonic and Phonon Effects

Sergey Kudryashov *, Pavel Danilov, Nikita Smirnov, Alexey Gorevoy, Volodymyr Kovalov

Posted Date: 7 September 2023

doi: 10.20944/preprints202309.0519.v1

Keywords: diamond; femtosecond laser; transmission spectra; self-phase modulation broadening; Bragg gratings; electron-hole plasma; nanoplasmonics; electron-phonon thermalization

Communication

Periodical Ultramodulation of Broadened Laser Spectra in Diamond at Variable Ultrashort Laser Pulsewidths: Ultrafast Plasma, Plasmonic and Phonon Effects

Sergey Kudryashov *, Pavel Danilov, Nikita Smirnov, Alexey Gorevoy and Volodymyr Kovalov

Lebedev Physical Institute, 119991 Moscow, Russia; danilovpa@lebedev.ru (P.D.); smirnovna@lebedev.ru (N.S.); a.gorevoy@lebedev.ru (A.G.); kovalevvy@lebedev.ru (V.K.)
* Correspondence: kudryashovsi@lebedev.ru (S.K.)

Abstract: Self-phase modulation (SPM) broadening of laser spectra was studied in a transmission mode in natural and synthetic diamonds at variable laser wavelengths (515 and 1030 nm), pulse energies and widths (0.3 - 12 ps, positively chirped pulses), providing their filamentary propagation. Besides the monotonous SPM broadening of the laser spectra versus pulse energy, more pronounced for the (sub)picosecond pulsewiths and more doped natural diamond, periodical low-frequency modulation was observed in the spectra at the shorter laser pulsewidths, indicating dynamic Bragg filtering of the supercontinuum due to ultrafast plasma and nanoplasmonic effects. Damping of broadening and ultramodulation for the longer picosecond pulsewidths was related to thermalized electron-hole plasma regime established for the laser pulsewidths longer, than 2 ps. Unexpectedly, at higher pulse energies and corresponding longer microfilaments, the number of spectral modulation features increases, indicating dynamic variation of the periods in the longitudinal plasma Bragg gratings along the filaments due to prompt secondary laser-plasmon interactions.

Keywords: diamond; femtosecond laser; transmission spectra; self-phase modulation broadening; Bragg gratings; electron-hole plasma; nanoplasmonics; electron-phonon thermalization

1. Introduction

Tight (numerical aperture NA > 0.3) focusing of ultrashort (femto – or picosecond, fs/ps) laser pulses in bulk dielectrics was approved as a key-enabling process in laser inscription of functional embedded optical or microfluidic elements [1–3]. This high-NA laser inscription regime provides in the focal region high enough peak laser intensities for the threshold-like optical breakdown (near-critical electron-hole plasma formation) and sufficient energy density deposition [4]. The photogenerated near-critical electron-hole plasma (EHP) promptly reduces the real part of local effective dielectric function of the photoexcited dielectric material, $Re\{\varepsilon^*\}$, down to zero (by definition of the critical plasma frequency and density). This makes possible intra-pulse laser excitation of interfacial plasmon-polaritons at the interface between the photoexcited (dielectric function ε^*) and unexcited dielectric (dielectric function ε) for $Re\{\varepsilon^*\} = \varepsilon_1^* + i\varepsilon_2^* \leq -Re\{\varepsilon\} = \varepsilon_1 + i\varepsilon_2$ with $\varepsilon_2 \approx 0$ [5,6]. The accompanying interference between the incident laser radiation and the induced interfacial electromagnetic waves strongly modulates the electric field and plasma density distributions in the interaction focal region; however, such near-or even sub-wavelength modulations of plasma density are hardly resolvable by optical imaging or diffraction methods, typically used for probing laser-generated plasma in dielectrics [7–9]. Non-linear focusing of ultrashort laser pulses via Kerr and Raman-Kerr effects and their resulting channeling makes the plasma and related plasmonic paths considerably elongated in the pre-focal region and potentially more pronounced in the underlying

Preprints (www.preprints.org) | NOT PEER-REVIEWED | Posted: 7 September 2023 doi:10.20944/preprints202309.0519.v1

laser propagation, spectral and structural effects, with the typical plasma densities in the near-critical range [4,6] due to NA-dependent scaling [10].

Moreover, during the last decade fs/ps-laser damage tracks in dielectrics were intentionally characterized in their cross-sections at high magnification by electron [11–14] and atomic force microscopy [6,15]. Such cross-sectional analysis revealed complex, regular and hierarchical structure of the damage features, typically emerging on sub- and near-wavelength spatial scales and related to laser interference phenomena, accompanied by nanoplasmonic interactions [6,15–18]. Though laser propagation regimes – geometrical (linear) focusing or filamentation (non-linear focusing) – were not identified in most of these previous studies, laser energy flow characteristics are rather monotonous, comparing to their modulation via interferential laser-plasmon interactions in the plasma channels [4,19,20]. These promising potential indications of nanoplasmonic processes during laser-dielectric interactions call for new enlightening experimental and theoretical studies.

In this study, optical transmittance spectra of ultrashort (0.3 - 12 ps) laser pulses at 515- and 1030-nm wavelengths and variable pulse energy were acquired in the pre- and filamentation regimes in bulk natural and synthetic diamonds to search for the first time in situ for spectral signatures of dynamic electron-hole plasma density modulation related to non-local laser-plasmonic interactions.

2. Materials and Methods

Diamond samples used in this studies were cubes (dimensions – 2 × 2 × 2 mm) with six polished opposite facets. The first sample was a IaB-type natural diamond (total nitrogen content - 190 ppm), while the second one was a pure IIa-type synthetic diamond (total nitrogen content <1 ppm).

Their transmission spectra were examined, employing ultrashort laser pulses at the central 1030-nm (fundamental, FH) and 515-nm (second harmonic, SH) wavelengths of a Yb-laser Satsuma (Amplitude Systemes, St. Etienne, France), corresponding to the spectral full-widths at the half-maximum of 2.7 and 1.3 nm, respectively. The FH and SH ultrashort laser pulses were precisely focused within the crystal volume at the refractive-index corrected 400-μm depth , using a micro-objective with a numerical aperture NA = 0.25, to yield the focal spot radius at the 1/e-intensity level ≤ 4 and 2 μm, respectively. Their pulsewidths were varied at the maintained bandwidth shape via partial positive chirping (incomplete back-compression of pre-stretched pulses upon amplification) in the range τ=0.3 - 12 ps, measured by means of a single-pulse auto-correlator AA-10DD-12PS (Avesta Project Ltd., Moscow, Russia). In the transmission studies, laser pulse energy was adjusted, using a thin-film transmissive attenuator (Standa, Vilnius, Lithuania), in the ranges E=50 - 5000 nJ (FH) and E=50 - 800 nJ (SH). The transmitted FH or SH radiation was collected by a 0.2-NA quartz/fluorite microscope objective (LOMO, St. Petersburg, Russia) and directed to the entrance slit of a spectrometer ASP-IR-2.5 (spectral range - 0.9 - 2.5 μm) or ASP-190 (spectral range – 190 - 1100 nm), both manufactured by Avesta Project Ltd., Moscow, Russia (Figure 1). Spectra were accumulated over a 10-second duration at the ultrashort laser pulse repetition rate of 10 kHz, while for the measurement at different pulse energies the samples were moved in steps by 50 μm, using a motorized translation stage for micro-positioning (Standa, Vilnius, Lithuania) after each spectrum acquisition.

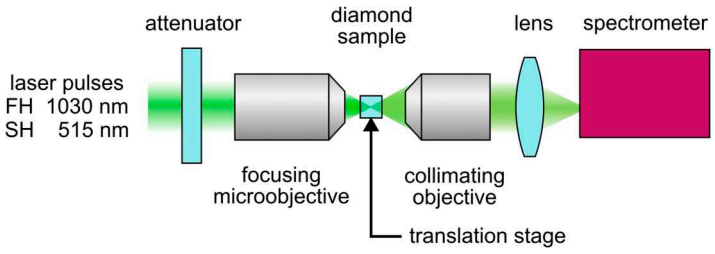

Figure 1. Experimental scheme for spectral acquisition of transmitted laser pulses.

Peak power and energy of ultrashort laser pulses were identified as critical parameters for filamentation in synthetic diamond samples. The onset of visible asymmetric elongation of glowing

Preprints (www.preprints.org) | NOT PEER-REVIEWED | Posted: 7 September 2023 doi:10.20944/preprints202309.0519.v1

filamentation channels towards laser radiation was observed as a function of increasing laser pulse energy (peak power), as previously reported [21,22]. This observation suggested the formation of a nonlinear focus beyond the Rayleigh length (linear focus parameter). For linearly polarized ultrashort laser pulses with a wavelength of 515 nm and varying pulse durations, the threshold energy values were discovered to be in the range of ≈210 - 230 nJ [21,22].

3. Results

3.1. Effect of nitrogen impurity

Direct comparison of the transmittance spectra of the 1030-nm laser pulses through the synthetic and natural diamonds at the same focusing and pulse energy conditions demonstrates the more pronounced – approximately by 3-10 times (depending on the laser pulsewidth) – spectral modulation for the latter sample (Figure 2). In the natural diamond, the onset of visible filamentation (plasma channel emission) occurs near 50 nJ, while in the synthetic diamond it starts near 300 nJ. Above the filamentation threshold, the number of Stokes and anti-Stokes sideband peaks monotonously increases, approaching, e.g., to 3 for the natural diamond versus 1 for the synthetic one at the 0.3-ps pulsewidth (Figure 2a), while to 3 for the natural diamond versus 1 for the synthetic one at the 0.6-ps pulsewidth (Figure 2b). The obvious reason is the presence of the intermediate stationary nitrogen-impurity states (absorption wavelength range - 330-410 nm, N3-center absorption [23]), rather than virtual states, in the bandgap of the natural diamond, strongly enhancing the optical nonlinearities via such intermediate resonances.

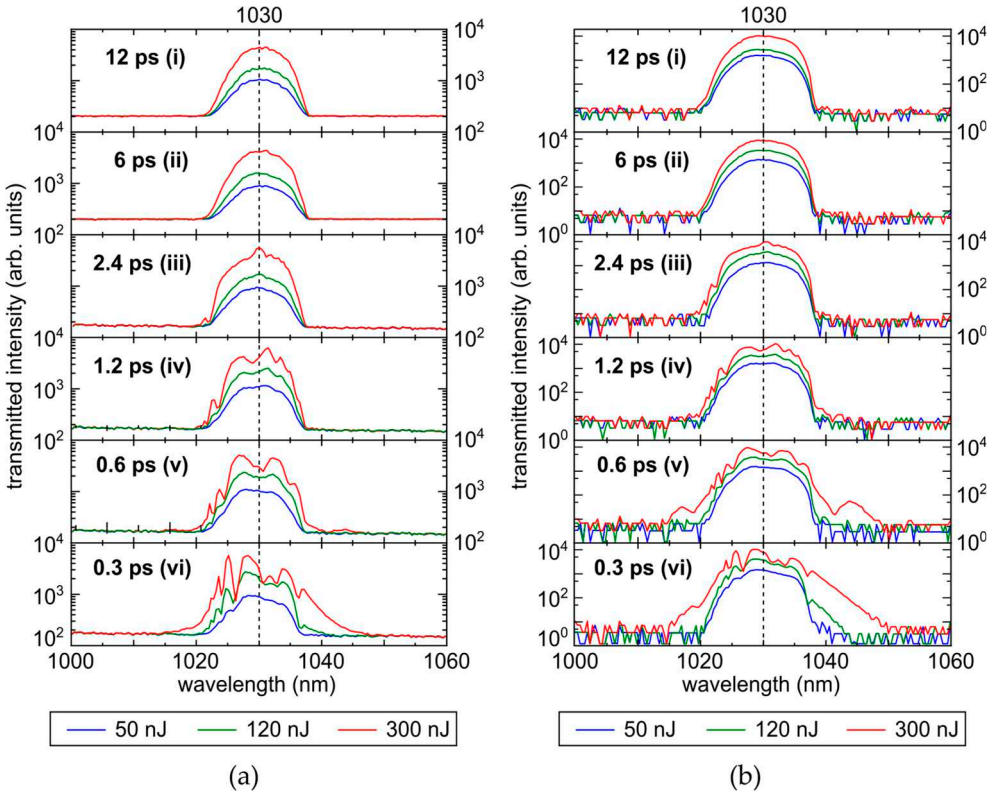

Figure 2. Comparative transmittance spectra of 1030-nm pulses at the different pulse energies (50, 120 and 300 nJ) and pulsewidths (i-vi) for the synthetic (a) and natural (b) diamond samples.

3.2. Effect of pulsewidth

In the synthetic diamond the 1030-nm transmitted pulses exhibit broader and stronger modulated spectra for the pulsewidth, increasing from 0.3 ps till 0.6 ps (Figures 2 and 3), with the following pulse elongation resulting in the spectral narrowing till the minimal width at 6 and 12 ps. Likewise, the 515-nm transmitted pulses in the diamond sample exhibit the same character of spectral

Preprints (www.preprints.org) | NOT PEER-REVIEWED | Posted: 7 September 2023 doi:10.20944/preprints202309.0519.v1

broadening dependence on the pulsewidth (Figure 4). In the natural diamond, at much lower pulse energies this trend is also present, but remains less pronounced (Figure 2).

Previously, such pulsewidth-dependent broadening of ultrashort-laser pulses was related to Kerr-like self-phase modulation and EHP screening, enhanced for the longer (picosecond) pulsewidths by Raman-Kerr effect [24,25]. The two former contributions are directly driven by pulse energy/pulsewidth ratio, however, the latter, Raman-Kerr contribution induced, e.g., by prompt excitation of coherent optical phonons [26,27], could appear on a picosecond timescale as a pulsewidth-invariant energy threshold value [21]. Meanwhile, at later picosecond times such nonlinear polarization related to optical phonons, should be damped by anharmonic decay of optical phonons into pairs of acoustic ones via the Clemens mechanism [28], being facilitated by the electron-phonon thermalization after 2 - 3 ps [29]. These picosecond effects in spectral broadening of ultrashort laser pulses and related lattice effects were recently overviewed in [25].

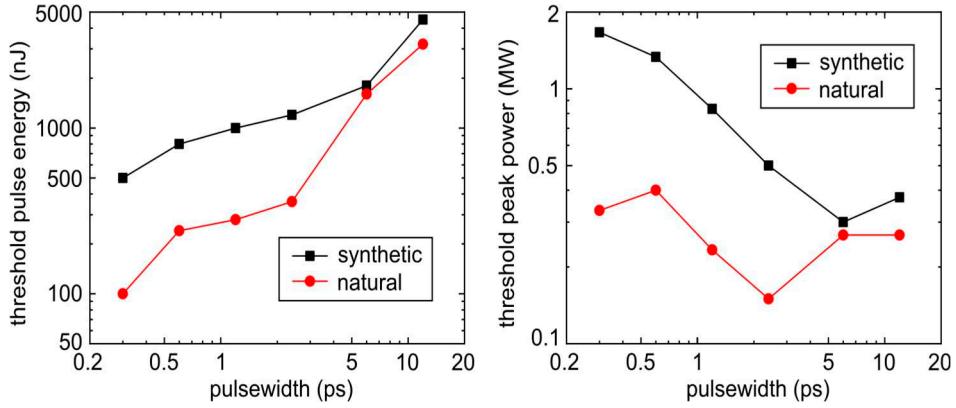

Figure 3. Threshold pulse energy and peak pulse power for the filamentation onset for 1030-nm pulses in the synthetic and natural diamond samples as a function of laser pulsewidth. Relative error bars – 10%.

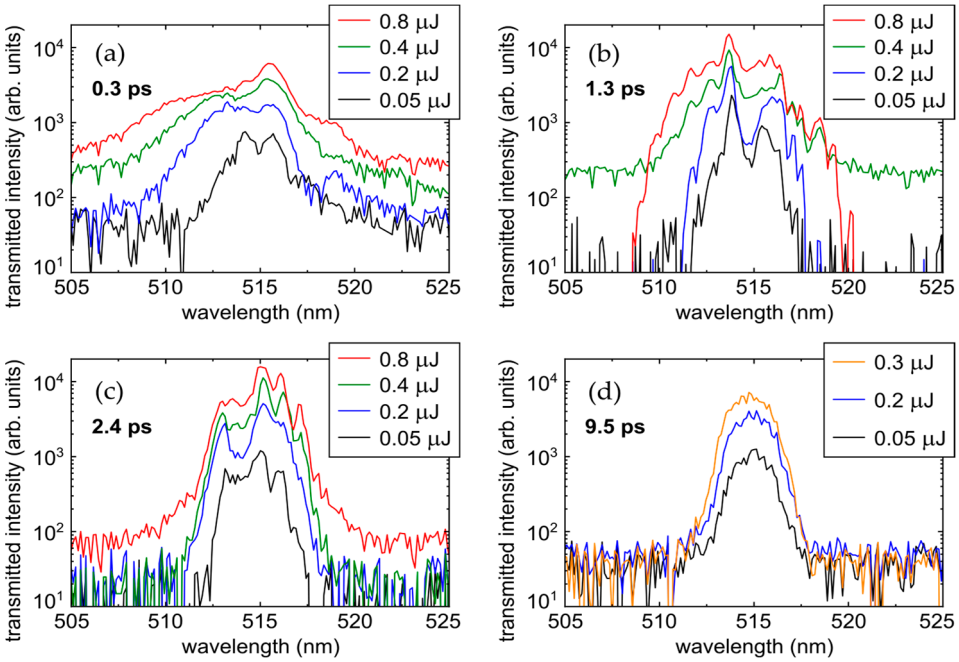

Figure 4. Transmittance spectra of 515-nm pulses at the different pulse energies and pulsewidths (a-d) for the synthetic diamond sample.

Preprints (www.preprints.org) | NOT PEER-REVIEWED | Posted: 7 September 2023 doi:10.20944/preprints202309.0519.v1

3.3. Effect of pulse energy

The pulse energy emerges as the most crucial parameter, governing the spectral broadening and modulation in the diamonds. In this study, by increasing the 1030-nm pulse energy magnitude till 5 μJ, unprecedently broad and strong modulation could be achieved for the pulsewidths, shorter or equal to 2.4 ps (Figure 5), with the number of sideband peaks approaching to ≈20 (above the noise level).

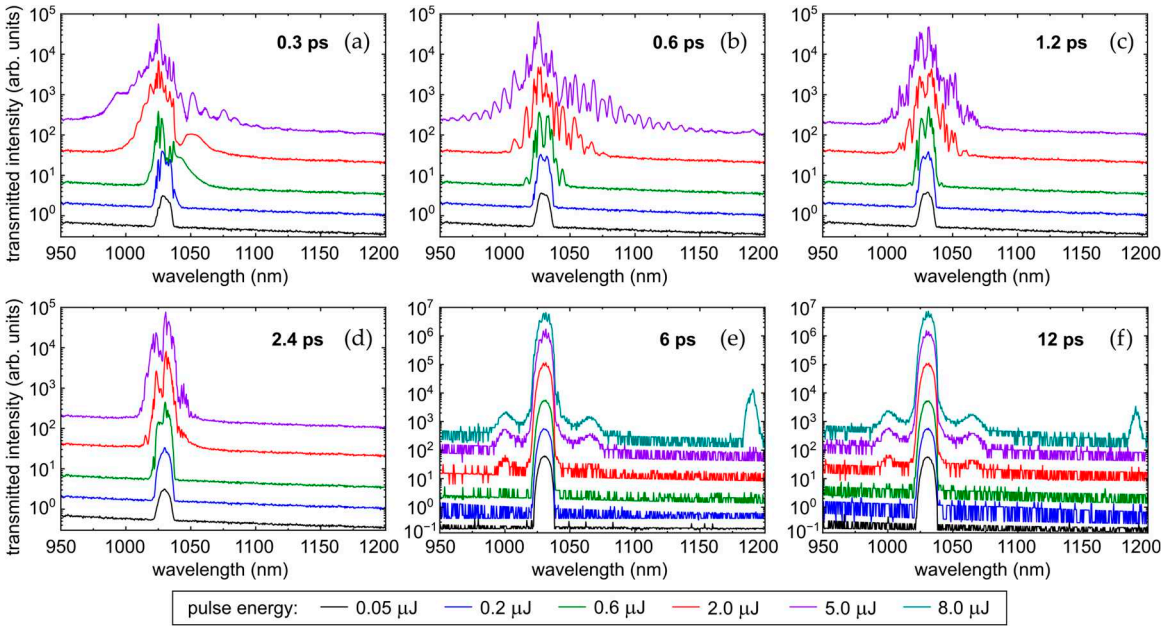

Figure 5. Transmittance spectra of 1030-nm pulses at the different pulse energies (color curves, see legend below) and pulsewidths (a-f) for the synthetic diamond sample. The spectra for different pulse energies are shifted along the vertical axis for clarity.

3.4. Effect of wavelength

Since we observe the pronounced spectral broadening and modulation in the diamond samples in the filamentation regime, the laser wavelength effect will influence these spectral changes via wavelength dependence of Kerr coefficient $n_2(\lambda)$ or critical power $P_{cr}(\lambda)$ for self-focusing [19],

$$P_{cr}(\lambda) \approx \frac{3.72}{8\pi} \frac{\lambda^2}{n_0(\lambda) n_2(\lambda)}, \quad (1)$$

i.e., in our experiments – via wavelength-dependent variation of the filamentation threshold energy. Obviously, according to Figure 3 and our previous studies [24], such filamentation threshold energy is much lower at the shorter laser wavelengths and thus more pronounced laser filamentation could be observed (the quantitative aspects will be discussed in the next section).

4. Discussion

Previously, such strongly broadened (supercontinuum, SC [19]) and modulated spectra were already observed for ultrashort – picosecond and femtosecond – laser pulses in transparent condensed media in the filamentation regime [30,31]. The periodical modulation, maximal at the both or one of shoulders of the self-phase modulation broadened spectra, was assigned to constructive or destructive interference of the new generated, phase-shifted spectral components [30].

In our study, surprisingly, no dominating shoulder peaks were observed, with the sideband intensities monotonously decreasing for the larger spectral shifts from the central laser wavelength, while the overall spectral width was monotonously increased versus laser pulse energy. As a result,

Preprints (www.preprints.org) | NOT PEER-REVIEWED | Posted: 7 September 2023 doi:10.20944/preprints202309.0519.v1

we were tempted to consider an alternative model of the ultramodulation in the SC spectra presented below.

First, we considered the observed filamentation of the ultrashort laser pulses within the "moving-foci" approach [19] (Figure 6), rather than their filamentary channeling. However, the plasma channels produced at the high-NA focusing and multi-TW/cm^2 laser intensities, contained near-critical or even supercritical EHP with the local density N_{cr}(1030 nm) ~ 1×10^{21} cm^{-3} at the 1030-nm wavelength and N_{cr}(515 nm) ~ 4×10^{22} cm^{-3} at the 515-nm wavelength for the refractive index of the plasma in the diamond n* ~ 1 (would be n^2-fold higher in unexcited diamond for its refractive index n(515,1030nm) ≈ 2.4 [32]), appearing during the self-focusing beam collapse as highly reflective, rather than refractive, like in gases [19].

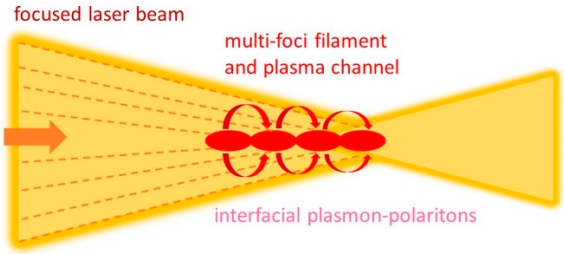

Figure 6. Schematic view of laser filaments ("moving-foci" regime [19]) with the supercritical EHP and plasmon-polariton excitation on their interface.

Meanwhile, the supercritical EHP density ($N_e > N_{cr}$, Re{ε*} < 0) in the filamentary plasma channels is required for laser excitation of plasmon-polaritons at the plasma channel interface with the surrounding less excited dielectric, according to the threshold condition Re{ε*} ≤ – Re{ε} [33] (Figure 7). Owing to the uncertainty of the self-focusing collapse arrest by the EHP regarding the final laser incidence angle on the plasma channel and other details, the corresponding plasmon-polaritonic dispersion curves were simulated for the filamentary channel with the supercritical EHP at different tentative self-focusing angles (0, 30, 45 and 60^0), using the common equations for the plasmon-polariton wavenumber $q(\omega)$ [34] under the crude approximation of a flat conductive interface and p-polarized laser radiation [33,35]

$$q_P(\omega) \approx \frac{\omega}{c}\left\{\sqrt{\frac{\varepsilon^*\varepsilon}{\varepsilon^*+\varepsilon}} \pm \sin\theta\right\} \tag{2}$$

where the corresponding expressions for the imaginary magnitudes ε* and ε with Re{ε*,ε} ~ Im{ε*,ε}, representing the lossy EHP in the dielectric, see in [33]. In fact, the exact solutions for excitation of longitudinal plasmon-polaritons in subwavelength metallic nanowire-channels (radius aω/c«1) correspond to qualitatively similar dispersion curves h(ω) of surfaces plasmon-polaritons (specifically, with similar asymptotic dispersion trends at h → 0 and h → ∞ [34]), some of which are overviewed in the book [35].

This means that non-linear spectral interactions (SC and harmonics generation etc.) could occur not only in the self-focusing beam, but also in the plasmonic field along the plasma channel, thus becoming considerably enhanced in longer filaments, alike in "channeling" filamentation regime.

Preprints (www.preprints.org) | NOT PEER-REVIEWED | Posted: 7 September 2023 doi:10.20944/preprints202309.0519.v1

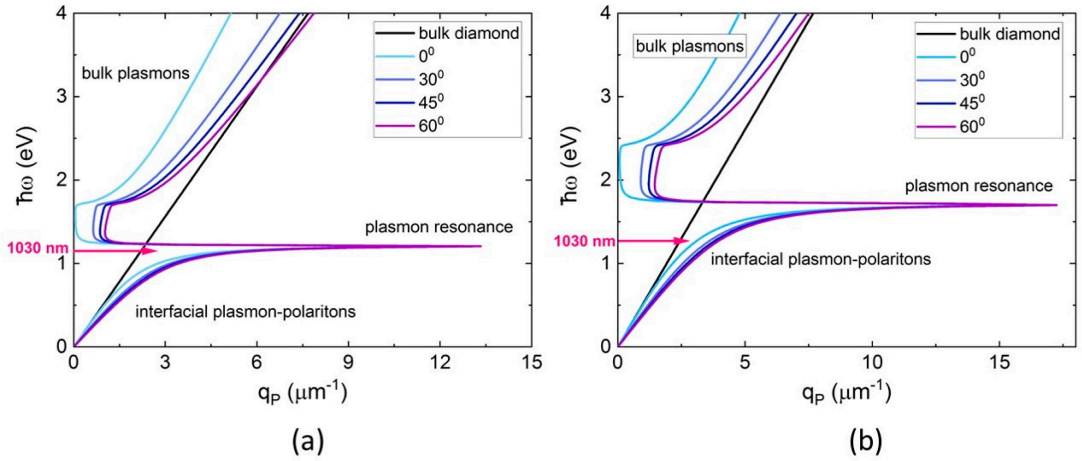

Figure 7. Dispersion curves of interfacial plasmon-polaritons, excited by 1030-nm fs-laser pulses in diamond at the incidence angles of 0, 30, 45 and 60⁰ on the interface "diamond-EHP" at supercritical EHP densities $N_e \approx 2\times10^{21}$ cm^{-3} (a) and $N_e \approx 4\times10^{21}$ cm^{-3} (b). The bulk electromagnetic wave dispersion line is denoted as "bulk diamond".

Second, prompt interference between the self-focusing laser radiation and interfacial plasmon-polaritons on the plasma channel interface provides their longitudinal interferential electric field patterns along the channels. Their potential periods are $1/q_P \sim \lambda/10$ (plasmon resonance in Figure 7) or $\sim\lambda$ (plasmon-polaritonic curves near the light-cone line $\omega=cq/n$), similarly to laser generation of periodical surface structures (LIPSS) on material surfaces [18,36]. Hence, an additional periodical modulation of plasma density (δN_e) and refractive index (δn^*) emerges in the periodical electric-filed "hot spots" in the filamentary plasma channels, which could work as a longitudinal Bragg grating to filter spectral components at the wavelengths Λ_{filt} [37]

$$\Lambda_{filt} \approx \frac{4\pi n_{eff}}{q_P}, \tag{3}$$

for the effective refractive index in the filament

$$n_{eff} \approx \frac{n^*(n^* + \delta n^*)}{n^* + (n^* + \delta n^*)}, \tag{4}$$

In the plasma channel with the near-critical or supercritical EHP density $n^* < n$, $n^*+\delta n^* \le n^*$ with $2n_{eff} < n$, thus, in many dielectrics $2n_{eff} \sim 1$, though variation of n^* near the critical EHP density is sharp and extensive (from $n^* \sim n$ till $n^* \ll 1$ in the supercritical EHP). Comparing to the expected plasmon-polariton wavelength for the flat metal/dielectric interface [18,36] in Eq.(2), one could find $q_P \approx 1/\lambda$ and thus $\Lambda_{filt} \approx \lambda$. This is consistent with our observations of the strongly modulated SC spectra around the central laser wavelength, which upon normalization to the SC intensity could be represented as the common Bragg-grating transmittance spectra (Figure 8). The multiple modulation in this case results not from multiple orders, but from the limited longitudinal number of grating stripes along the plasma channels.

Preprints (www.preprints.org) | NOT PEER-REVIEWED | Posted: 7 September 2023 doi:10.20944/preprints202309.0519.v1

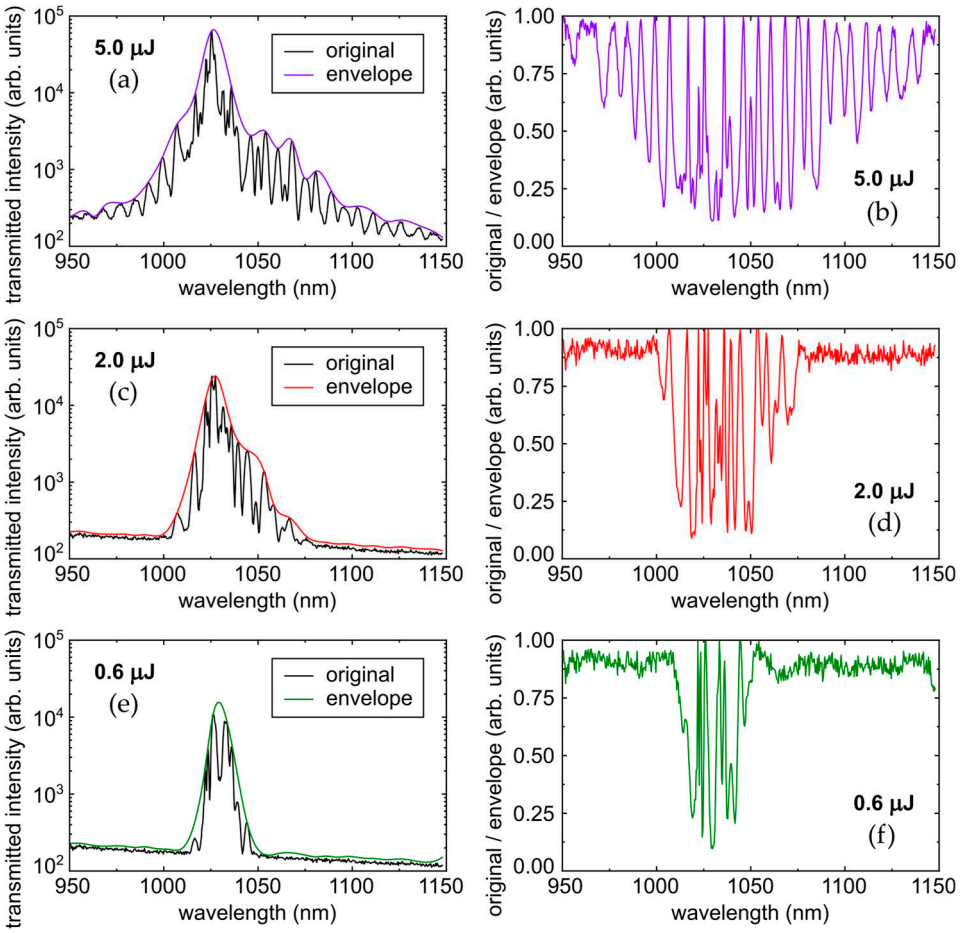

Figure 8. Transmitted intensity (a,c,e) and transmittance (b,d,f) spectra of 0.6-ps 1030-nm pulses for the synthetic diamond sample: original spectra with the corresponding SC spectra (envelopes in a,c,e) and their ratio (b,d,f) at the different pulse energies (5.0, 2.0 and 0.6 μJ).

Counterintuitively, according to the common diffraction theory, the higher pulse energies in Figure 5 result in the longer filaments and, potentially, the larger longitudinal numbers of regularly-spaced grating stripes along the plasma channels and more pronounced central minimum with less distinct side minima. However, in our spectral experiments at the higher pulse energies (pulsewidth – 0.6 ps, Figure 8) we observed the increasing number of nearly equal, closely-spaced spectral modulation features, thus potentially indicating longitudinal non-uniformity of the Bragg grating periods. This could be a first indirect indication of non-local – e.g., plasmon-polariton propagation – effects along the plasma channels, accumulating plasmon-polariton energy deposition downstream the plasma channels and vice versa making the filaments/channels longitudinally non-uniform too.

5. Conclusions

Transmittance spectra of focused (NA = 0.25) ultrashort (0.3 - 12 ps) positively chirped laser pulses at 515- and 1030-nm wavelengths were acquired in the filamentation regime in natural and synthetic diamonds. Besides monotonous pulse energy-dependent self-phase modulation broadening of laser spectra (supercontinuum generation), becoming pronounced only in the filamentation regime for the laser pulsewidths shorter or equal to 2.4 ps, unusual periodical low-frequency modulation was observed in the spectra for the shorter laser pulsewidths. We suggested the occurrence of supercritical electron-hole plasma in the filaments, inducing plasmon-polariton excitation on their interface with the unexcited dielectric and resulting in nanoplasmonic modulation of plasma density. Then, dynamic filtering of the laser supercontinuum proceeds in the plasma Bragg gratings. Damping of spectral broadening and ultramodulation for the longer picosecond

pulsewidths was related to thermalized electron-hole plasma regime established for the laser pulsewidths longer, than 2 ps.

Author Contributions: Conceptualization, S.K.; project administration, funding acquisition, S.K.; writing—review and editing, S.K., A.G.; methodology, P.D., V.K.; validation, N.S.; formal analysis, A.G.; investigation, P.D., N.S.; data curation, V.K.; writing—original draft preparation, S.K.; supervision, S.K. All authors have read and agreed to the published version of the manuscript.

Funding: This research was funded by Russian Science Foundation, grant number 21-79-30063; https://rscf.ru/en/project/21-79-30063/ (accessed on April 04, 2023).

Data Availability Statement: Additional data could be provided by the authors upon a special request.

Conflicts of Interest: The authors declare no conflict of interest.

References

1. Sugioka, K.; Cheng, Y. Ultrafast Lasers-Reliable Tools for Advanced Materials Processing. *Light Sci. Appl.* **2014**, *3*, 149.
2. Sotillo, B.; Bharadwaj, V.; Hadden, J.P.; Sakakura, M.; Chiappini, A.; Fernandez, T.T.; Longhi, S.; Jedrkiewicz, O.; Shimotsuma, Y.; Criante, L.; et al. Diamond photonics platform enabled by femtosecond laser writing. *Sci. Rep.* **2016**, *6*, 35566.
3. Kudryashov, S.; Danilov, P.; Smirnov, N.; Kuzmin, E.; Rupasov, A.; Khmelnitsky, R.; ... Gorevoy, A. Photoluminescent Microbit Inscripion Inside Dielectric Crystals by Ultrashort Laser Pulses for Archival Applications. *Micromachines* **2023**, *14*(7), 1300.
4. Couairon, A.; Sudrie, L.; Franco, M.; Prade, B.; Mysyrowicz, A. Filamentation and damage in fused silica induced by tightly focused femtosecond laser pulses. *Phys. Rev. B* **2005**, *71*, 125435.
5. Klimov, V. *Nanoplasmonics*. CRC press, Singapore, 2014.
6. Kudryashov, S.; Rupasov, A.; Kosobokov, M.; Akhmatkhanov, A.; Krasin, G.; Danilov, P.; Lisjikh, B.; Abramov, A.; Greshnyakov, E.; Kuzmin, E.; et al. Hierarchical Multi-Scale Coupled Periodical Photonic and Plasmonic Nanopatterns Inscribed by Femtosecond Laser Pulses in Lithium Niobate. *Nanomaterials* **2022**, *12*, 4303.
7. Mouskeftaras, A.; Rode, A.V.; Clady, R.; Sentis, M.; Utéza, O.; Grojo, D. Self-limited underdense microplasmas in bulk silicon induced by ultrashort laser pulses. *Applied Physics Letters* **2014**, *105*(19), 191103.
8. Papazoglou, D.G.; Abdollahpour, D.; Tzortzakis, S. Ultrafast electron and material dynamics following femtosecond filamentation induced excitation of transparent solids. *Applied Physics A* **2014**, *114*, 161-168.
9. Jürgens, P.; Vrakking, M.J.J.; Husakou, A.; Stoian, R.; Mermillod-Blondin, A. Plasma formation and relaxation dynamics in fused silica driven by femtosecond short-wavelength infrared laser pulses. *Applied Physics Letters* **2019**, *115*(19), 191903.
10. Geints, Y.E.; Zemlyanov, A.A.; Ionin, A.A.; Kudryashov, S.I.; Seleznev, L.V.; Sinitsyn, D.V.; Sunchugasheva, E.S. Peculiarities of filamentation of sharply focused ultrashort laser pulses in air. *J. Exp. Theor. Phys.* **2010**, *111*, 724–730.
11. Song, J.; Wang, X.; Hu, X.; Dai, Y.; Qiu, J.; Cheng, Y.; Xu, Z. Formation mechanism of self-organized voids in dielectrics induced by tightly focused femtosecond laser pulses. *Appl. Phys. Lett.* **2008**, *92*, 092904.
12. Li, X.; Xu, J.; Lin, Z.; Qi, J.; Wang, P.; Chu, W.; Fang, Z.; Wang, Z.; Chai, Z.; Cheng, Y. Polarization-insensitive space-selective etching in fused silica induced by picosecond laser irradiation. *Appl. Surf. Sci.* **2019**, *485*, 188–193.
13. Xu, S.; Fan, H.; Li, Z.-Z.; Hua, J.-G.; Yu, Y.-H.; Wang, L.; Chen, Q.-D.; Sun, H.-B. Ultrafast laser-inscribed nanogratings in sapphire for geometric phase elements. *Opt. Lett.* **2021**, *46*, 536–539.
14. Zhang, B.; Liu, X.; Qiu, J. Single femtosecond laser beam induced nanogratings in transparent media—Mechanisms and applications. *J. Mater.* **2019**, *5*, 1–14.
15. Kudryashov, S.; Rupasov, A.; Zakoldaev, R.; Smaev, M.; Kuchmizhak, A.; Zolot'ko, A.; Kosobokov, M.; Akhmatkhanov, A.; Shur, V. Nanohydrodynamic Local Compaction and Nanoplasmonic Form-Birefringence Inscription by Ultrashort Laser Pulses in Nanoporous Fused Silica. *Nanomaterials* **2022**, *12*, 3613.
16. Shimotsuma, Y.; Kazansky, P.G.; Qiu, J.; Hirao, K. Self-organized nanogratings in glass irradiated by ultrashort light pulses. *Phys Rev Lett* **2003**, 91, 247405.
17. Taylor, R.; Hnatovsky, C.; Simova E. Applications of femtosecond laser induced self-organized planar nanocracks inside fused silica glass. Laser Photon Rev. **2008**, 2, 26-46.
18. Kudryashov, S.I.; Danilov, P.A.; Rupasov, A.E.; Smayev, M.P.; Kirichenko, A.N.; Smirnov, N.A.; Ionin, A.A.; Zolot'ko, A.S.; Zakoldaev, R.A. Birefringent microstructures in bulk fluorite produced by ultrafast pulsewidth-dependent laser inscription. *Appl. Surf. Sci.* **2021**, *568*, 150877.

19. Couairon, A.; Mysyrowicz, A. Femtosecond filamentation in transparent media. *Phys. Rep.* **2007**, 441, 47–189.
20. Kudryashov, S.I.; Samokhvalov, A.A.; Geints, Y.E.; Ageev, E.I.; Veiko, V. P. Femtosecond laser filaments in gold colloidal solutions: supercontinuum and ultrasonic tracing. *JOSA B* **2019**., *36*(2), A125-A130.
21. Kudryashov, S.; Krasin, G.; Rupasov, A.; Danilov, P.; Kosobokov, M.; Akhmatkhanov, A.; Lisjikh, B.; Turygin, A.; Greshnyakov, E.; Kovalev, M.; et al. Ferroelectric nanodomain engineering in bulk lithium niobate crystals in ultrashort-pulse laser nanopatterning regime. *Nanomaterials* **2022**, *12*, 4147.
22. Krasin, G.K.; Gulina, Y.S.; Kuzmin, E.V.; Martovitskii, V.P.; Kudryashov, S.I. Polarization-Sensitive Nonlinear Optical Interaction of Ultrashort Laser Pulses with HPHT Diamond. *Photonics* **2023**, *10*, 106.
23. Zaitsev, A.M. *Optical properties of diamond: a data handbook*; Springer Berlin, Heidelberg: Berlin, Germany, 2013.
24. Kudryashov, S.I.; Danilov, P.A.; Kuzmin, E.V.; Gulina, Y.S.; Rupasov, A.E.; Krasin, G.K.; Zubarev, I.G.; Levchenko, A.O.; Kovalev, M.S.; Pakholchuk, P.P.; Ostrikov, S.A.; Ionin, A.A. Pulse-width-dependent critical power for self-focusing of ultrashort laser pulses in bulk dielectrics. *Opt. Lett.* **2022**, *47*, 3487–3490.
25. Kudryashov, S.; Danilov, P.; Chen, J. Intrapulse correlated dynamics of self-phase modulation and spontaneous Raman scattering in synthetic diamond excited and probed by positively chirped ultrashort laser pulses. *Photonics* **2023**, *10*, 626.
26. Ishioka, K.; Hase, M.; Kitajima, M.; Petek, H. Coherent optical phonons in diamond. *Applied Physics Letters* **2006,** *89*(*23*), 231916.
27. Zukerstein, M.; Kozák, M.; Trojánek, F.; Malý, P. Experimental observation of anharmonic effects in coherent phonon dynamics in diamond. *Diamond and Related Materials* **2018**, *90*, 202-206.
28. Klemens, P.G. Anharmonic decay of optical phonon in diamond. *Phys. Rev. B* **1975**, *11*, 3206.
29. Kudryashov, S.; Danilov, P.; Smirnov, N.; Krasin, G.; Khmelnitskii, R.; Kovalchuk, O.; Kriulina, G.; Martovitskiy, V.; Lednev, V.; Sdvizhenskii, P.; et al. "Stealth Scripts": Ultrashort Pulse Laser Luminescent Microscale Encoding of Bulk Diamonds via Ultrafast Multi-Scale Atomistic Structural Transformations. *Nanomaterials* **2023**, *13*, 192.
30. Shen, Y.R. *The Principles of Nonlinear Optics*; Wiley-Interscience: New York, NY, USA, 1984.
31. Grudtsyn, Y.V.; Zubarev, I.G.; Koribut, A.V.; Kuchik, I.E.; Mamaev, S.B.; Mikheev, L.D.; Semjonov, S.L.; Stepanov, S.G.; Trofimov, V.A.; Yalovoi, V.I. Self-Phase modulation in a thin fused silica plate upon interaction with a converging beam of down-chirped femtosecond radiation. *Quantum Electron.* **2015**, *45*, 415–420.
32. Palik, E.D. *Handbook of Optical Constants of Solids*; Academic Press: Orlando, USA, 1998.
33. Bell, R.J.; Alexander, R.W. Jr.; Parks, W.F.; Kovener, G. Surface excitations in absorbing media. *Opt. Commun.* **1973**, *8*, 147–150.
34. Guo, X.; Ma, Y.; Wang, Y.; Tong, L. Nanowire plasmonic waveguides, circuits and devices. *Laser & Photonics Reviews* **2013**, *7*(6), 855-881.
35. Prokhorov, A.M.; Sychugov, V.A.; Tishchenko, A.V.; Khakimov, A.A. *Sov. Tech. Phys. Lett.* **1982**, *8*, 605.
36. Kudryashov, S.I.; Nastulyavichus, A.A.; Saraeva, I.N.; Rudenko, A.A.; Zayarny, D.A.; Ionin, A.A. Deeply sub-wavelength laser nanopatterning of Si surface in dielectric fluids: Manipulation by surface plasmon resonance. *Appl. Surf. Sci.* **2020**, *519*, 146204.
37. Bak, J.; Suazo Betancourt, J.L.; Rekhy, A.; Abbasszadehrad, A.; Miles, R.B.; Limbach, C.M.; Walker, M.L. High resolution spatially extended 1D laser scattering diagnostics using volume Bragg grating notch filters. *Review of Scientific Instruments* **2023**, *94*(2), 023003.